http://dx.doi.org/10.5012/bkcs.2012.33.4.1141

The Characteristics of YAG:Ce Phosphor Powder Prepared Using a NO_3^--Malonic Acid-NH_4NO_3-$NH_3 \cdot H_2O$ System

Jin An Jeong, Kyunghwan Park,[†] Dong Hoon Lee,[‡] Hong Gun Kim,[#] and Yoo Young Kim[§,*]

NJS Cablecar Co., Jeongeup, Jeonbuk 580-300, Korea
[†]Jeonju University High School, Jeonju, Jeonbuk 560-860, Korea
[‡]Tech4M Co., Suwon, Gyeonggi-do 443-803, Korea
[§]Department of Mechanical and Automotive Engineering, Jeonju University, Jeonju, Jeonbuk 560-759, Korea
[*]E-mail: yooykim@jj.ac.kr
[#]Department of Nano and Advanced Materials Engineering, Jeonju University, Jeonju, Jeonbuk 560-759, Korea
Received April 11, 2011, Accepted December 21, 2011

Ce-doped $Y_3Al_5O_{12}$ (YAG:Ce) phosphor powder was prepared using a NO_3^--malonic acid-NH_4NO_3-$NH_3 \cdot H_2O$ system. The YAG:Ce precursor was ignited at 240 ºC and the resulting powder contained YAG:Ce crystallites (42%) - active in the visible region at 460 nm - amorphous particles (53%) - inactive at visible wavelengths - and less than 3% oxide (3%) crystallite impurities. The impurities transformed to acitive YAG:Ce crystallites at above 800 ºC. At above 1000 ºC, the amorphous phase became YAG phase and isolated Ce_2O crystallites emerged. The powder particles comprised < 4 μm secondary aggregates of 20 nm primary particles. The thermal dusting of the secondary particles coincided with the aggregation of the secondary particles at above 900 ºC.

Key Words : YAG:Ce phosphor, Combustion method, Malonic acid

Introduction

Phosphorescent $Y_3Al_5O_{12}$:Ce (YAG:Ce) is thermally and chemically stable and has good mechanical properties and high luminescence. It gives bright yellow emission at 530 nm under blue excitation at 460 nm, giving it applicability in white light emitting diodes (LEDs) through combination with blue LEDs.[1] Such luminescent properties are due to electronic transitions between the 4f and 5d orbitals of Ce^{3+} ions located at distorted cubic site in the YAG matrix,[2] suggesting photoluminescence depends on the amount of visible-active Ce^{3+} ions.

YAG:Ce phosphor powders have been prepared by solid state reaction[3,4] and by solution methods such as sol-gel,[5,6] co-precipitation,[7-9] spray dry,[10] spray pyrolysis,[11,12] and combustion[13-16] technique. This works reports the preparation of the YAG:Ce phosphor powder from the combustion of malonate ($^-OOCCH_2COO^-$) oxidant and nitrate (NO_3^-) fuel. The preparation of mixed oxides using the NO_3^--malonic acid-NH_4NO_3-$NH_3 \cdot H_2O$ system (e.g. $CoAl_2O_4$,[17] $MgAl_2O_4$[18]) has advantages of generating concentrated combustion heat - due to the quick combustion of the mixed oxide precursors - that can drive mixed oxide crystallite synthesis, and of uniformly distributing metal cations in the prepared precursor. Non-uniformly distributed metallic cations can lead to parent oxides in the resulting powder. This system's advantages indicate its suitability for the production of phosphorescent YAG:Ce powder. The incorporation of the only Ce^{3+} ions into YAG matrices leads to photo-luminescent properties at 460 nm. Then, Ce ions can be ether tri- or tetra-valent. Under atmospheric conditions phosphorescent YAG:Ce powder will be prepared using the sources of Ce^{3+} rather than those of Ce^{4+}, since incorporation of Ce^{4+} requires a reducing atmosphere. Cerium nitrate hexahydrate was used as the source of Ce^{3+} in this work.

MAl_2O_4 (M = Co^{2+}, Mg^{2+}) powders that were prepared using this system were composed of the product crystallites and the amorphous substance.[17,18] Also, at above 1300 ºC, the amorphous substance was converted into MAl_2O_4 crystallites, i.e. the single crystalline phase was obtained. Then, the YAG:Ce phosphor powder prepared by this system would have the two phases: the crystalline and the amorphous phases. This work was of interest in the two facts. The one fact was the fraction of the crystalline phase in the prepared powder. The other was whether the amorphous phase had the photo-luminescent property or not. The YAG:Ce precursor was prepared using the NO_3^--malonic acid-NH_4NO_3-$NH_3 \cdot H_2O$ system and it was ignited at 240 ºC and the resulting powder was characterized by the X-ray diffratometry (XRD), thermo-gravimetry and differential thermal analysis (TG/DTA), Fourier transformation infrared spectroscopy, Brunauer-Emmett-Teller (BET) measurement, ultraviolet-visible (UV-vis) spectroscopy and scanning electron microscopy (SEM).

Experimental

Preparation and Ignition of Precursor. Yttrium oxide (Y_2O_3), aluminum nitrate nonahydrate ($Al(NO_3)_3 \cdot 9H_2O$), cerium nitrate hexahydrate ($Ce(NO_3)_3 \cdot 6H_2O$), and ammonium nitrate (NH_4NO_3) were roughly mixed and concentrated ammonia water was added. The mixture was mechanically

mixed for 20 min, left at room temperature for 12 hr and dried at 80 °C and 25 torr until it formed a paste. The paste was solidified at 100 °C for 12 hr, heated at 140 °C for 1 hr in air and then evacuated at 140 °C and 10^{-3} torr. The heating and evacuation were repeated three times. The final mixture was ignited at 240 °C on the previously prepared YAG:Ce powder. The resulting powder was labeled the sample powder.

0.15 mole sample powder was produced from: 0.21825 mole of Y_2O_3 (99.9%, Daejung, Korea), 0.0135 mole of $Ce(NO_3)_3{\cdot}6H_2O$ (99.99%, Kanto, Japan), 0.7500 mole of $Al(NO_3)_3{\cdot}9H_2O$ (98%, Daejung), 0.6000 mole of NH_4NO_3 (98%, Duksan, Korea), 0.8093 mole of malonic acid (Junsei, Japan) and *ca.* 90 mL of concentrated ammonia water (27.2%, Duksan). The batch formula on this composition was $(Y_{2.91}Ce_{0.09})Al_5O_{12}$.

Separation of the Sample Powder by Distilled Water. 80 g sample powder was ball-milled in 300 mL distilled water for 24 hr, transferred to a 500 mL beaker and the resulting upper colloid, containing water and some sample powder, was decanted after 1 hr. The upper colloid was used to recover powders after sedimentation for 6 and 24 hr. The three separated powders were heated at 300 °C in air for 3 hr. Hereafter, the powder with 1 hr of sedimentation time will be referred to as the P01 powder, and so on. The powders were labeled by their hours of sedimentation: P01, P06 and P24, their yield are listed in Table 1.

Powders' High-Temperature Heat-Treatment. P01 and the sample powders were heated at 2 °C/min and 5 hr in air. The resulting powders were ball-milled in air for three days.

Characterization of Precursor and Powders. The prepared precursor and the obtained powders were examined by X-ray powder diffraction (XRD) using a MAC Science MXP^3 system with a copper target. The X-ray tube voltage was 40 kV and the current was 10 mA. Diffraction patterns were recorded over a 2θ range of 10-80° with a 0.04° step-size at 0.5 s/step. The intensity and FWHM (full width at half maximum) of the (420) peak (the largest peak attributable to the YAG phase) were obtained using the diffractometer's software from XRD patterns recorded with 2θ steps of 0.002° at 0.5 sec/step. Constant mass was used to obviate mass effect. Average particle sizes ($D_{X\text{-}ray}$) were calculated using the Scherrer equation:

$$D_{hkl} = \frac{K\lambda}{\beta_{hkl}\cos\theta} \quad (1)$$

Table 1. Yields, specific surface areas (σ), and FWHMs of the (420) peaks for P01, P06 and P24 powders. Average particle sizes were calculated by equation (1) and (2)

Powder	Yield /%	σ/$m^2{\cdot}g^{-1}$	FWHM /degree	Particle size/nm	
				D_{BET}	D_{hkl}
Sample		12.11	0.494	110	16.6
P-01	77.8	5.55	0.418	240	19.6
P-06	14.7	7.15	0.420	186	19.6
P-24	4.5	9.42	0.430	142	19.1

where K is a constant (normally 0.89), λ is the wavelength of the incident X-ray's radiation (here 0.15418 nm), β_{hkl} is the peak's FWHM in radians and θ is a half of 2θ, the position of the diffraction in radians.

The thermal behavior of the prepared precursor was assessed by the thermogravimetry (TG) and differential thermal analysis (DTA) with a MAC Science TG/DTA 2000. Heating was at 10 °C/min between 100 and 500 °C. The reference material was α-Al_2O_3.

Malonate and nitrate anions in the prepared precursor were examined by infrared spectroscopy. FT/IR spectrum was obtained at room temperature on the JASCO FT/IR 5300 spectrophotometer between 400 and 4600 cm^{-1} at 2 cm^{-1} resolution using KBr pellet.

The powders' absorptivities were estimated from their 460 nm absorbance signal in the UV-vis reflectance spectra, which were recorded at 350-600 nm on a Varian Cary 500 spectrophotometer with a resolution of 0.5 nm. Each spectrum's base line was corrected using the tangent-line technique and the background was then subtracted.

Emission and excitation spectra were obtained using a Hitachi F-4500 spectrofluorimeter.

Powders' surface areas were assessed through BET measurement on a Qunatachrome Autosorb-1 after the powders were degassed at 230 °C for 6 hr. Assuming cubic particles, their average particle sizes (D_{BET}) were calculated by Eq. (2):

$$D_{BET} = \frac{6}{D_x \cdot \sigma} \quad (2)$$

where σ is the specific surface area of the prepared powder and D_x is the theoretical density of YAG (4.551 g/cm^3).

The powders' morphologies were observed by SEM images recorded on a JEOL JSM-7500F.

Results and Discussion

Precursor Characterization. X-ray diffraction showed the prepared precursor to be mainly amorphous (Figure 1(a)). The precursor's FT/IR spectrum (Figure 2) shows two strong absorption bands between 1200 and 1800 cm^{-1}: a singlet at 1604 cm^{-1} and another band at 1385 cm^{-1} with a shoulder at 1470 cm^{-1}. The band at 1604 cm^{-1} was attributed to C=O stretching in the carboxylate anion ($-COO^-$), the shoulder at 1470 cm^{-1} to CH_2 vibrations in the malonate anion. The spectrum showed that the hydrogenmalonate anions ($HOOCCH_2COO^-$) were not present in the prepared precursor. The vibrational energy of the C=O groups was found to be *ca.* 20 cm^{-1} higher than those in metal malonate hydrate.[19,20] The band at 1385 cm^{-1} was assigned to NO_3^- anion.[21,22] Figure 1(a) and Figure 2 show that the specific malonate salts of yttrium and aluminum were not isolated in the prepared precursor. The TG/DTA thermogram (Figure 3) shows that the nitrate and malonate salts were uniformly distributed in the precursor. The precursor showed single-step decomposition at 250-278 °C, with the heat of decomposition being emitted on this range. Such decomposition

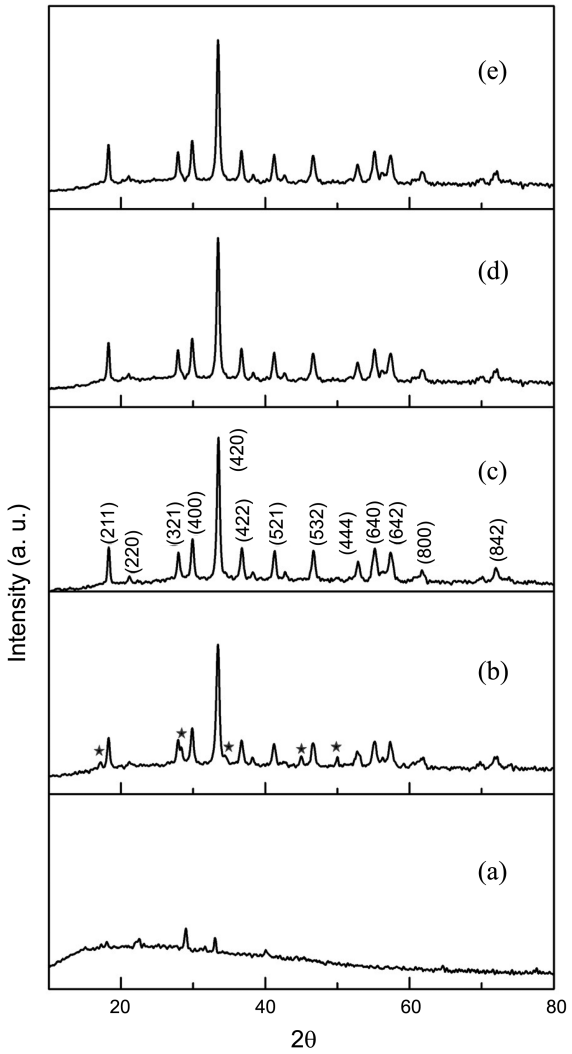

Figure 1. X-ray diffraction patterns of the (a) precursor (b) sample, (c) P01, (d) P06 and (e) P24 powders. ★ denotes peaks attributed to the impurity phase.

characteristics of decomposition demonstrates that the salts in the prepared precursor were uniformly distributed.

X-Ray Diffraction Patterns. The powders' XRD patterns (Figure 1(b)-(e)) show P01, P06 and P24 exhibited peaks due to the YAG phase (JCPDS No. 33-0040) and that the sample powder exhibited peaks due to the YAG phase and an impurity phase. Impurity particles adhered to the surfaces of P01, P06 and P24 particles (Figure 1(b)). The summation of the yields powders P01, P06 and P24 was 97% (Table 1), indicating overall impurities in the sample powder at below 3%.

XRD patterns recorded after the separate heating of the sample powder and P01 (Figure 4(a) and (b)) show decreasing impurity peaks shown by the sample powder at above 800 °C, which disappeared by 1000 °C. The intensity of a diffraction peak generally represents the content of the crystallites assigned to it. Therefore, the intensity of (420) peak, the largest peak in the YAG phase, was examined with respect to the preparation temperature of the sample powder (Figure 5). The peak's intensities clearly increased at 800-

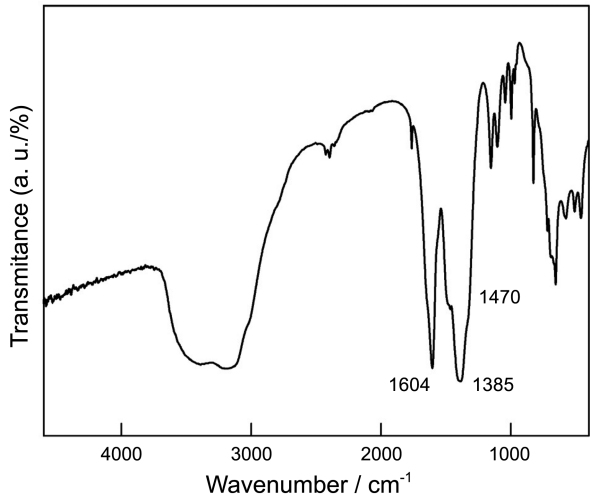

Figure 2. FT/IR spectrum of the prepared precursor.

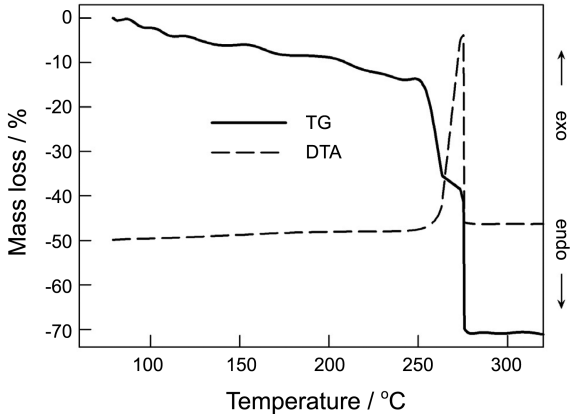

Figure 3. TG/DTA thermogram of the prepared precursor.

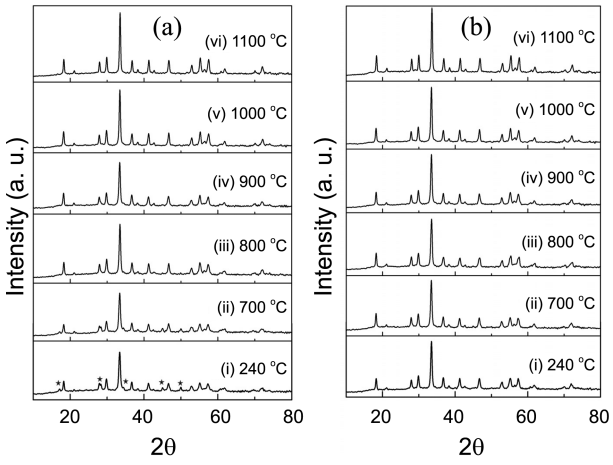

Figure 4. X-ray diffraction patterns of powders obtained from the (a) sample and (b) P-01.

1000 °C, indicating increasing YAG phase concentration, in line with Figure 4(a-iii), and showing that the impurity phase transformed into YAG phase at increased temperatures of powder preparation.

The intensity increment at 1000 °C shown by P01 (Figure 5(b)) represents increased formation of YAG crystallites

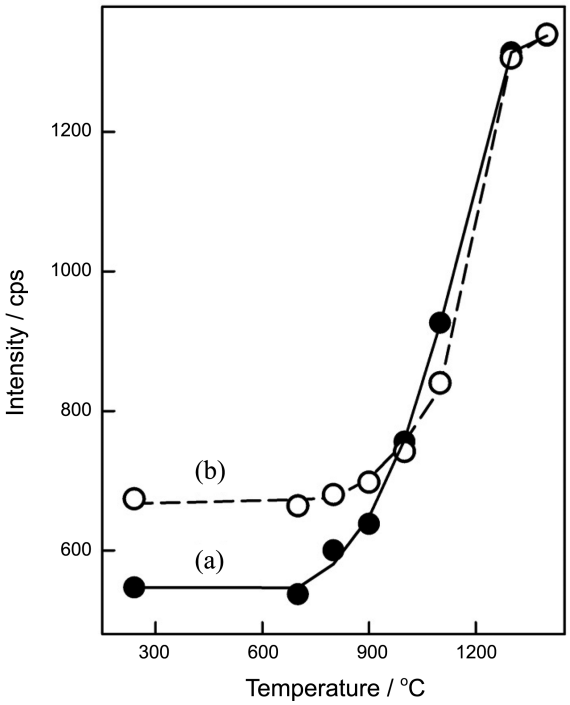

Figure 5. Intensities of the (420) peaks of powders prepared from the (a) sample and (b) P01.

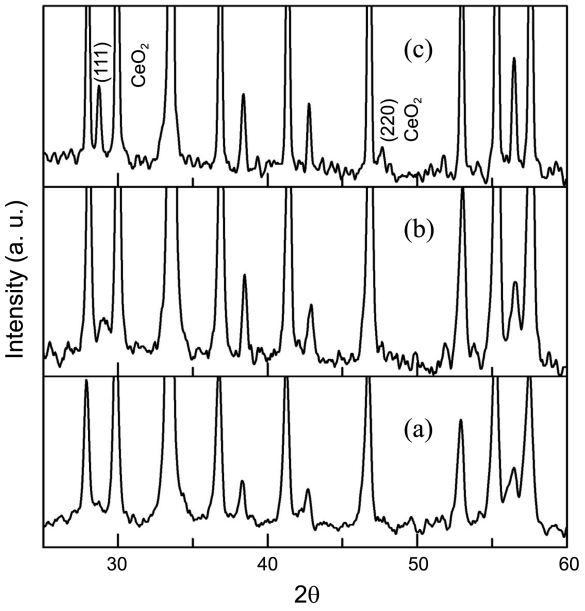

Figure 6. X-ray diffraction patterns of powders prepared from P01 at (a) 1000, (b) 1100 and (c) 1300 °C around a baseline

rather than amorphous phase, at the increased preparation temperature, since P01 did not show impurity signals. P01's amorphous phase was transformed into YAG crystallites at above 1000 °C. The behavior of Ce ions in the amorphous phase was studied during its transformation into YAG phase. (111) and (220) peaks, the two most prominent assigned to the CeO_2 phase (JCPDS No. 34-0394), were clearly shown by the powder obtained from P01 at 1300 °C (Figure 6), demonstrating that Ce ions in the amorphous phase were not

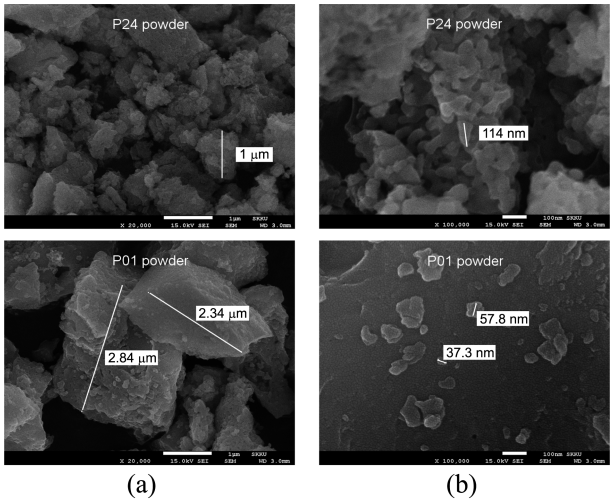

Figure 7. SEM images, with (a) 20,000 × and (b) 100,000 × magnification, of P01 and P24. The (a) and (b) scale-bars size are 1 μm and 100 nm, respectively.

incorporated into the YAG matrix during its transformation into YAG crystallites. Mancic *et al.*[11] reported that cerium dioxide phase was present in YAG:Ce powder prepared at 1000 °C via spray pyrolysis.

Two intensities of (420) peaks at 1300 °C were similar (Figure 5), i.e. the contents of the crystalline phase in the two powders were identical. And the intensities of (420) peaks at 1400 °C were slightly larger than those at 1300 °C. It was considered that this intensity change with the increasing temperature was due to the sintered effect of powder. Therefore, the intensities at 1300 °C could be the reference value to estimate the contents of the YAG:Ce crystallites in the sample powder and P01: 42% for the sample powder and 51% for P01 powder.

Particles' Size and Morphology. SEM images of powders P01 and P24 (Figure 7) show that P01 was composed of irregularly shaped particles of several micrometers. Nanoparticles were observed on the surfaces of the micro-sized particles in the magnified image of P01. P24, with the longer sedimentation time, comprised mainly particles of *ca.* 100 nm, with some particles of below 2 μm. The powders' specific surface areas (σ) agree with these results, with the σ of P24 (9.42 m^2/g) being larger than that of P01 (5.55 m^2/g). The particle sizes of P01, P06 and P24 were calculated using equation (1) and (2) and are listed in Table 1. The average particle sizes calculated using equation (1) were below 20 nm, while those from equation (2) were 140-240 nm, demonstrating that the sample powder was composed of secondary particles formed from the aggregates of primary particles.

SEM images of the powders prepared at high temperatures from P01 show that the secondary particles prepared at 900 and 1100 °C were smaller than those prepared at 700 °C. Dusting of the secondary particles occurred at above 900 °C. Although the XRD result shows that the transformation of the amorphous phase to YAG phase occurred at above 1000 °C, this transformation may have led to the dusting of

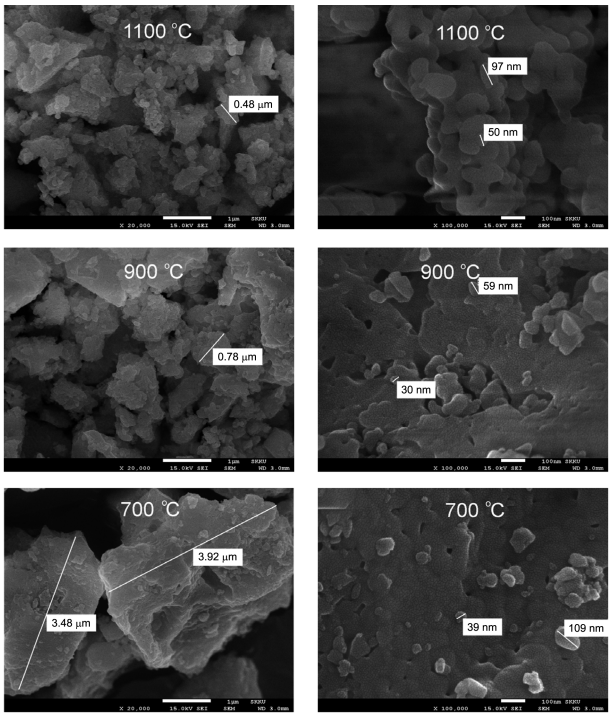

Figure 8. SEM images, with (a) 20,000 × and (b) 100,000 × magnification, of powders prepared from P01. The (a) and (b) scale-bars size are 1 μm and 100 nm, respectively.

the secondary particles at 900 °C. It may be not meaningful to examine the morphology of the particles prepared at 1100 °C, since CeO_2 crystallites were isolated with the transformation of the amorphous phase. However, the powder prepared at 1100 °C comprised aggregates of the dusted particles.

UV-vis Reflectance and Photo-luminescent Spectra. UV-vis reflectance spectra of the sample powder and the powders obtained from it at high temperatures (Figure 9) each show maximum absorbances (λ_{max}) at 460 nm. The sample powder showed the smallest λ_{max}, indicating that its impurity phase was indicative at visible wavelengths. The powder prepared at 900 °C showed a greater λ_{max} than the sample powder because at above 900 °C, the inactive impurity phase transformed into YAG crystallites, which were active in the visible region. The sample prepared at 1100 °C showed a similar λ_{max} to that prepared at 900 °C because Ce ions in the amorphous phase were not incorporated into the YAG matrix during the transformation from amorphous to YAG phase at above 1000 °C, indicating that the Ce ions in the amorphous phase were inactive at visible wavelengths and that the visible-active YAG crystallites formed during the combustion of the prepared precursor and also that the impurity phase were stable at high temperature. The powders' contents of YAG and impurity-phase crystallites, which formed during the combustion of the prepared precursor, determined their photoluminescent performance.

The powder prepared from the sample powder at 900 °C

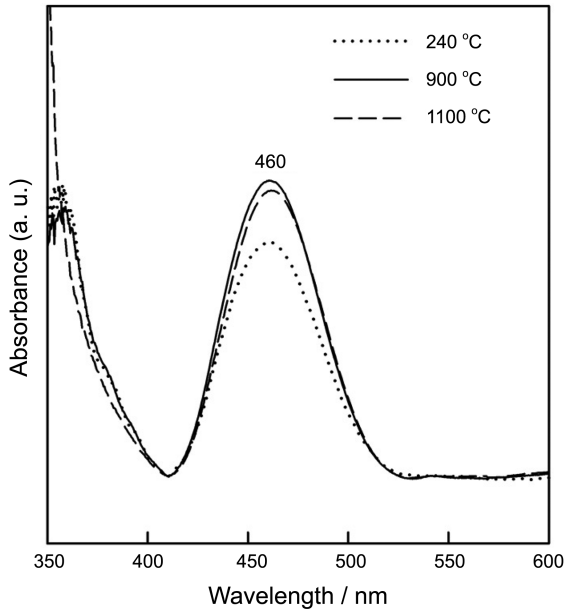

Figure 9. UV-vis reflectance spectra of the sample powder and powders obtained from it.

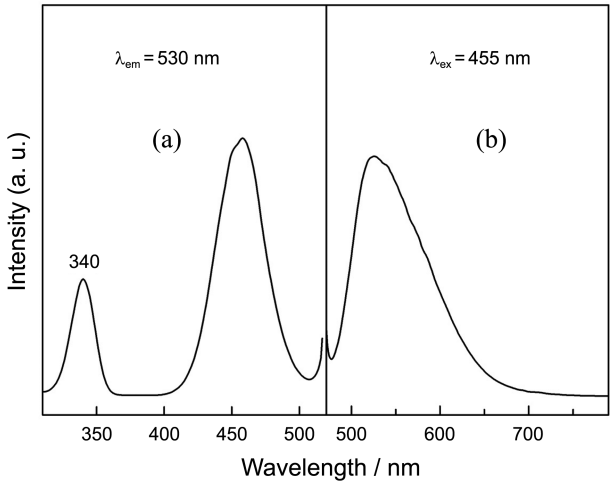

Figure 10. (a) Emission and (b) excitation spectra of powder prepared from the sample powder at 900 °C.

showed a 4f → 5d transition of Ce ions at 455 nm in its excitation spectrum (Figure (a)) and emission at 530 nm from this excitation in its emission spectrum (Figure 10(b)).

Conclusion

YAG:Ce precursor was prepared using a NO_3^--malonic acid-NH_4NO_3-$NH_3{\cdot}H_2O$ system. Its combustion, ignited at 240 °C, produced powders comprising YAG:Ce crystallites, active at visible wavelengths, and inactive amorphous phase and impurity crystallites. The impurity crystallites transformed into the visible-active YAG crystallites at above 800 °C and the amorphous phase transformed into the YAG phase, with concurrent isolation of Ce_2O crystallites, at above 1000 °C. The Ce ions in the amorphous phase were not active at visible wavelengths. The visible-active YAG

crystallites formed during the combustion of the prepared precursor and those formed from the impurity phase were stable at high temperature. The contents of YAG and impurity crystallites that formed during the combustion of the precursor determined the photoluminescent performance of the final powder.

The powder produced from the combustion of the precursor mainly comprised particles of several micrometers that as secondary aggregates of primary nanoparticles. The aggregated were thermally dusted at above 900 °C. The powder sintered at 900 °C was shown to be best for the preparation of fine YAG:Ce phosphor powders.

Conclusionally, the amount of the active YAG:Ce crystallites at visible wavelengths in the resulting powder from the YAG:Ce precursor should be increased. In order to increase the photoluminescent performance of the prepared powder, the experimental conditions need to be improved, such as the amount of malonic acid, the pH of a mixture prior to dryness, the molar ratio of malonic acid to the nitrate anion, the addition of the crystallization accelerator in the YAG:Ce precursor, the time schedule of combustion, etc.

Acknowledgments. Authors thank Prof. Y. R. Kim, Department of Chemistry, Yonsei University, for the measurement of the emission and excitation spectra.

References

1. Lee, S. H.; Jung, D. S.; Han, J. M.; Koo, H. Y.; Kang, Y. C. *J. Alloy. Compd*. **2009**, *477*, 776.
2. Blasse, G.; Bril, A. *J. Chem. Phys*. **1967**, *47*, 5139.
3. Tsai, M. S.; Fu, W. C.; Wu, W. C.; Chen, C. H.; Yang, C. H. *J. Alloys Compd*. **2008**, *455*, 461.
4. Huh, Y. D.; Cho, Y. S.; Do, Y. R. *Bull. Korean Chem. Soc*. **2002**, **23**, 1435.
5. Potdevin, A.; Chadeyron, G.; Boyer, D.; Mahiou, R. *J. Non-Cryst. Solids* **2006**, *352*, 2510.
6. Sun, Z.; Yuan, D.; Li, H.; Duan, X.; Sun, H.; Wang, Z.; Wei, X.; Xu, H.; Luan, C.; Xu, D.; Lv, M. *J. Alloy Compd.* **2004**, *379*, L1.
7. Han, R.; Wang, L.; Chen, K.; Yang, S. *Mater. Sci. Eng. B* **2010**, *166*, 41.
8. Saladino, M. L.; Caponetti, E.; Martino, D. C.; Enzo, S.; Ibba, G. *Opt. Mater*. **2008**, *31*, 261.
9. Palmero, P.; Esnouf, C.; Montanaro, L.; Fantozzi, G. *J. Eur. Ceram. Soc*. **2005**, *25*, 1565.
10. Lee, H. M.; Cheng, C. C.; Huang, C. Y. *Mater. Res. Bull.* **2009**, *44*, 1081.
11. Mancic, L.; Marinkovic, K.; Marinkovic, B. A.; Dramicanin, M.; Milosevic, O. *J. Euro. Ceram. Soc.* **2010**, *30*, 577.
12. Jung, K. Y.; Lee, H. W. *J. Lumin*. **2007**, *126*, 469.
13. Fadlalla, H. M. H.; Tang, C. C.; Elssfah, E. M.; Zhang, J.; Ammar, E.; Lin, J.; Ding, X. X. *Mater. Res. Bull.* **2008**, *43*, 3457.
14. Purwanto, A.; Wang, W. N.; Ogi, T.; Lenggoro, I. W.; Tanabe, E.; Okuyama, K. *J. Alloy Compd.* **2008**, *463*, 350.
15. Liu, X. J.; Li, H. L.; Xie, R. J.; Zeng, Y.; Huang, L. P. *J. Lumin.* **2007**, *124*, 75.
16. Xia, G.; Zhou, S.; Zhang, J.; Xu, J. *J. Crystal Growth* **2005**, *279*, 357.
17. Lee, G. Y.; Lee, D. H.; Kim, H. G.; Kim, Y. Y. *Bull Korean Chem. Soc.* **2010**, *31*, 47.
18. Jeong, J. A.; Kim, Y. Y. *Inst. Eng. Tech. Jeonju Univ.* **2010**, *15*, 55.
19. Brusau, E. V.; Narda, G. E.; Pedregosa, J. C.; Echeverria, G.; Punte, G. M. *J. Solid State Chem.* **1999**, *143*, 174.
20. Ristova, M.; Petrusevski, G.; Raskovska, A.; Soptrajanov, B. *J. Mol. Struct*. **2009**, *924*, 93.
21. Grzona, C. B.; Lick, I. D.; Castellon, E. R.; Ponzi, M. I.; Ponzi, E. N. *Mater. Chem. Phys.* **2010**, *123*, 557.
22. Tllez Soto, C. A.; Carauta, A. N. M.; de M. Carneiro, J. W. *Spectrochimica Acta A* **2009**, *71*, 1140.